



Amides Do Not Always Work: Observation of Guest Binding in an Amide-Functionalized Porous Metal–Organic Framework

Oguarabau Benson,[†] Ivan da Silva,[‡] Stephen P. Argent,[†] Rafel Cabot,[†] Mathew Savage,[§] Harry G.W. Godfrey,[§] Yong Yan,[§] Stewart F. Parker,[‡] Pascal Manuel,[‡] Matthew J. Lennox,[†] Tamoghna Mitra,^{†,⊥} Timothy L. Easun,^{†,||} William Lewis,[†] Alexander J. Blake,[†] Elena Besley,[†] Sihai Yang,^{*,§} and Martin Schröder^{*,§}

[†]School of Chemistry, University of Nottingham, Nottingham, NG7 2RD, U.K.

[‡]ISIS Facility, STFC Rutherford Appleton Laboratory, Chilton, Oxfordshire, OX11 0QX, U.K.

[§]School of Chemistry, University of Manchester, Manchester, M13 9PL, U.K.

^{||}School of Chemistry, Cardiff University, Cardiff, CF10 3XQ, U.K.

[⊥]Department of Chemistry, University of Liverpool, Liverpool, L69 7ZD, U.K.

S Supporting Information

ABSTRACT: An amide-functionalized metal organic framework (MOF) material, MFM-136, shows a high CO₂ uptake of 12.6 mmol g⁻¹ at 20 bar and 298 K. MFM-136 is the first example of an acylamide pyrimidyl isophthalate MOF without open metal sites and, thus, provides a unique platform to study guest binding, particularly the role of free amides. Neutron diffraction reveals that, surprisingly, there is no direct binding between the adsorbed CO₂/CH₄ molecules and the pendant amide group in the pore. This observation has been confirmed unambiguously by inelastic neutron spectroscopy. This suggests that introduction of functional groups solely may not necessarily induce specific guest–host binding in porous materials, but it is a combination of pore size, geometry, and functional group that leads to enhanced gas adsorption properties.

Recent developments in materials chemistry and crystal engineering have shown that metal–organic frameworks (MOFs) have promising properties that complement or compete favorably with zeolites and activated carbons in various applications.¹ MOFs are crystalline porous coordination polymers consisting of polyatomic organic ligands linked to metal ions/clusters by covalent bonds.² MOFs have shown great promise for gas adsorption and storage owing to their high porosity and internal surface area, and tunable functionality on the pore surface for selective gas binding. Generation of open metal sites³ and incorporation of pendant functional groups⁴ at the pore surface are two dominant methods of functionalizing MOF cavities. For example, MOFs with open Cu(II) sites can show strong adsorption affinity to molecular H₂.⁵ Recently, the detailed binding mechanisms to saturated and unsaturated light hydrocarbons have been rationalized in a hydroxyl-functionalized MOF.⁶ Within the field of carbon capture, materials functionalized with amines (–NH₂), imines (–NH), and amides (–CONH) dominate, largely because of their potential to form specific interactions

with CO₂, leading to highly selective CO₂ uptakes. Although high CO₂ adsorption has been observed in a number of amine-, imine- and amide-functionalized MOFs,⁷ molecular insight into the direct binding between adsorbed CO₂ molecules and porous host (especially toward these functional groups) is largely lacking. Recently, direct H₂N(δ–)⋯(δ+)CO₂ binding has been observed in a Zn(II) MOF incorporating amine groups that protrude into the pore, providing structural insight into the observed high CO₂ adsorption in this material.⁴

The incorporation of pendent amide (–CONH–) and/or amine groups into MOFs is thus regarded generally as a promising approach to enhance CO₂ uptake due to the formation of hydrogen bonds with amides serving as both hydrogen bond acceptors (via C=O) and donors (via N–H). A series of amide-functionalized MOFs have been synthesized and shown to exhibit high CO₂ uptakes and selectivities.^{7b,8} Likewise, computational studies attribute this to the specific binding and formation of hydrogen bonds between adsorbed CO₂ molecules and free amide or amine groups thus enhancing adsorption affinity and selectivity for CO₂.^{7c,8c,9} However, to date there are few physical investigations on the precise role of amides in CO₂ binding in MOFs. The challenge of such investigations is further increased in MOF systems containing open metal sites owing to the inevitable competition for guest binding between the open metal sites and the organic functional group(s) in the pore. Here, we report the synthesis, structure, and gas adsorption properties of an amide-functionalized pyrimidyl Cu(II)-isophthalate MOF, MFM-136, which shows a high CO₂ adsorption capacity (12.6 mmol g⁻¹ at 20 bar and 298 K). In MFM-136, all Cu(II) sites are fully coordinated to carboxylate and pyrimidyl groups, affording a pore environment without open metal sites. This gives an ideal environment for studying the binding interaction between amides and adsorbed CO₂ molecules since it eliminates the competitive binding of CO₂ on the open Cu(II) sites. In this situation, we can clearly evaluate the precise role of free amides

Received: August 3, 2016

Published: September 26, 2016

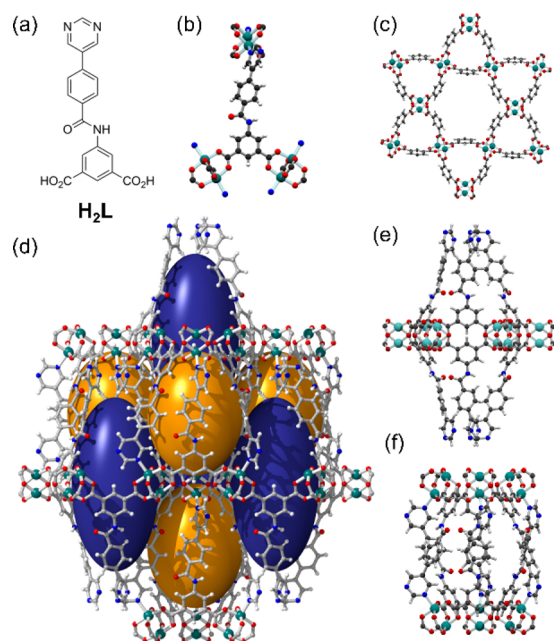


Figure 1. (a) Chemical structure of ligand H_2L . (b) Coordination environment of L^{2-} in MFM-136. (c) View along the c -axis of the Kagome lattice in MFM-136. (d) View of the alternate packing of large cages **A** (blue) and small cages **B** (orange) in MFM-136. Views of (e) the large cage **A** and (f) small cage **B** both along the b -axis. Colors: C, black; H, white; O, red; N, blue; Cu, teal.

in guest binding in the pore. Combined neutron diffraction and inelastic neutron spectroscopy have revealed the preferred binding sites for CO_2 in the pore and the corresponding host-guest binding dynamics. Surprisingly, there is no direct binding between adsorbed CO_2/CD_4 and free amides in this case. This is supported by grand canonical Monte Carlo (GCMC) simulations.

Solvothermal reaction of 5-[4-(pyrimidin-5-yl)benzamido]-isophthalic acid (H_2L , Figure 1a) with $Cu(NO_3)_2 \cdot 3H_2O$ in DMF at 80 °C for 16 h yields MFM-136 as green single crystals. MFM-136 crystallizes in space group $R32$ and shows a 3D binodal (3,6)-connected network with a rare *eea*-topology.^{8f,10} In MFM-136, the binuclear $[Cu_2(O_2CR)_4]$ paddlewheels coordinate to two pyrimidyl nitrogen atoms from two different ligands at both axial positions, resulting in the absence of open Cu(II) sites in the entire structure (Figure 1). The metal-ligand connectivity in MFM-136 affords two types of cages (**A** and **B**). Cage **A** is surrounded by 12 $[Cu_2(O_2CR)_4]$ paddlewheel units and six linkers and has a prolate-ellipsoid shape (length 24.9 Å, width 10.6 Å). Cage **B** is enclosed by six $[Cu_2(O_2CR)_4]$ paddlewheel units and six linkers and has a more spherical shape (length 16.2 Å, width 12.5 Å). The overall structure is an alternate packing of these two types of cages to give a highly porous and robust framework material with a void fraction of 54% and BET surface area of 1634 m² g⁻¹ (Figure S6).

At 273 K, the CO_2 sorption isotherms of desolvated MFM-136 show an uptake of 7.3 mmol g⁻¹ at 1 bar and 14.3 mmol g⁻¹ at 20 bar, representing the highest CO_2 uptake in monoamide-functionalized MOFs reported to date (Table S2). Methane adsorption in MFM-136 gives a lower uptake of 2.9 mmol g⁻¹ at 1 bar and 8.3 mmol g⁻¹ at 20 bar at 273 K. The experimental CO_2 adsorption isotherms show good agreement with grand canonical Monte Carlo (GCMC) simulations

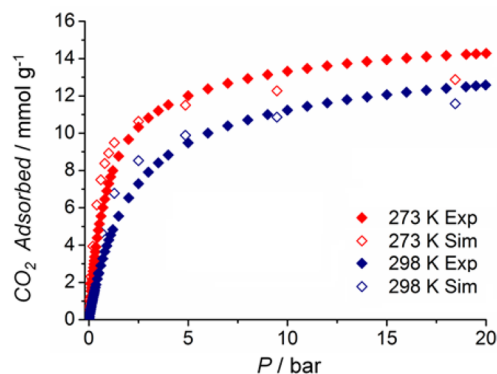


Figure 2. Experimental and simulated adsorption isotherms for CO_2 in desolvated MFM-136 at 273 and 298 K.

(Figure 2). In contrast, MFM-136 shows negligible N_2 uptake under the same conditions, leading to selectivities for CO_2/N_2 and CO_2/CH_4 of 27:1 and 6.3:1, respectively, at 273 K. The isosteric heats of adsorption for CO_2 and CH_4 in MFM-136 are calculated using the Virial method as 25.6 and 16.0 kJ mol⁻¹, respectively, at low surface coverage. The selective CO_2 uptake in MFM-136 is lower than the leading ultramicroporous MOFs,¹¹ however, the high capacity indicates MFM-136 remains a promising candidate in the separation of CO_2 over CH_4 and N_2 .¹² The lack of open Cu(II) sites in the pores of MFM-136 prevents strong binding to water molecules, which often triggers framework collapse or hydrolysis in MOFs containing open metal sites.¹³ Previously reported MOFs containing amides in the absence of open metal sites have exhibited high CO_2 capacities;¹⁴ however, the role of the amides in CO_2 binding was not defined structurally.

It is reported that the excellent uptake of CO_2 in amide-functionalized MOFs is a consequence of specific CO_2 -amide interactions based upon hydrogen bond formation between the amide $-NH(\delta^+)$ and the $O(\delta^-)$ of CO_2 .^{7c,8a} To gain experimental insight, preferred binding sites in MFM-136 have been determined by *in situ* neutron powder diffraction (NPD) as a function of gas loading (CO_2 and CD_4). NPD patterns were recorded at 7 K for the desolvated material and at loadings of 1.8 and 2.3 CO_2/Cu and 1.1 CD_4/Cu . Fourier difference map analysis of the NPD patterns revealed positions of the adsorbed CO_2 and CD_4 molecules, which were further developed by Rietveld refinement. All binding sites were checked carefully for their unambiguous presence in the final structural model; i.e., a parallel refinement without each of the binding sites was carried out to confirm the presence of each site by comparing the R factors and the residual peaks.

The NPD data at a loading of 1.8 CO_2/Cu reveals eight binding sites **A–H** distributed between cages **A** and **B** (Figure 3). The CO_2 molecules are constrained to be linear with equal C–O bond lengths, while their crystallographic occupancies and positions (including orientations) have been refined. At low CO_2 loading, adsorbate-adsorbate interactions will be negligible meaning that the site occupancies directly reflect the binding strength between CO_2 and the framework. Three CO_2 sites **A–C** have significantly higher occupancies (0.65, 0.44, and 0.40, respectively) than the remaining five sites **D–H** (ranging within 0.26–0.11); surprisingly none of the sites makes an apparent hydrogen bonding interaction with the amide moiety. Site **A** resides on a 3-fold symmetry axis in the center of a triangular pocket formed by a $[(Cu_2)_3(isophalate)_3]$ unit, where the CO_2 makes three identical long contacts to the phenyl rings

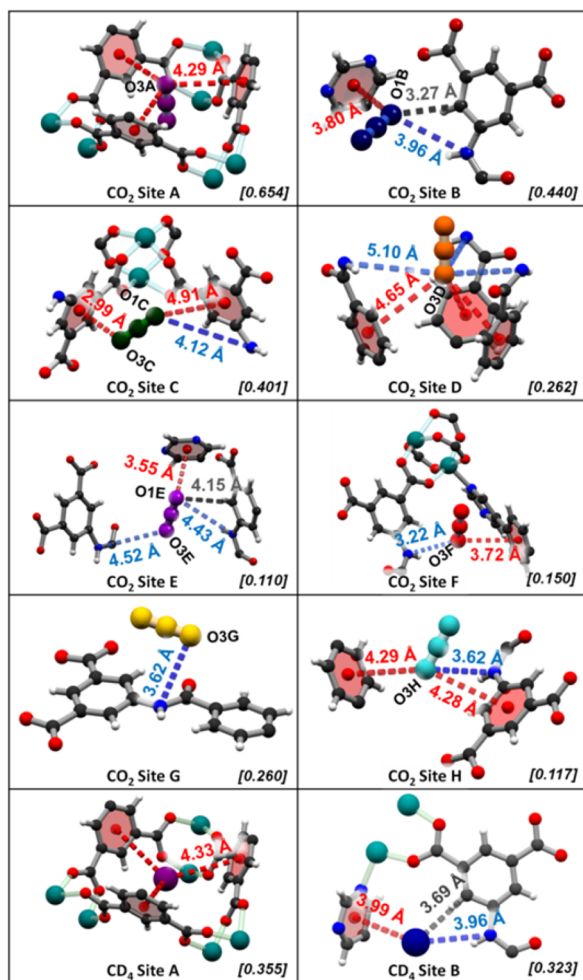


Figure 3. Binding sites of guests in MFM-136 at loadings of 1.8 CO₂/Cu(II) and 1.1 CD₄/Cu(II) elucidated from Rietveld refinement of NPD data. Colors: carbon, black; hydrogen, white; oxygen, red; nitrogen, blue; copper, teal; CO₂/CD₄ guests, purple/dark blue/green for sites A/B/C, respectively. Refined chemical occupancies of guest molecules inset.

[O1A_{CO₂}···ring centroid = 4.21(2) Å]. Site B lies close to a pyrimidine ring (O1B_{CO₂}···ring centroid = 3.22(9) Å) and makes a shorter contact with the aromatic C–H group on a phenyl ring (O1B_{CO₂}···C32 = 3.27(7) Å) along with a longer distance to an amide N–H (O1B_{CO₂}···N29 = 3.96(8) Å). Site C lies close to an isophalate phenyl ring (O3C_{CO₂}···ring centroid = 2.99(6) Å). The shortest contact between a guest CO₂ and amide nitrogen atom is observed for the low occupancy site F (occupancy = 0.15) where the guest accepts a weak hydrogen bond (N29···O3F_{CO₂} = 3.22(20) Å; < N–H···O = 122(5)°). The absence of CO₂ molecules adjacent to the uncoordinated pyrimidine nitrogen atom is not surprising, as the site is sterically hindered by a neighboring phenyl ring; however, no such impediment exists around the amide N–H site which is fully accessible to the guest molecules. The preference of CO₂ to make multiple long-range contacts with phenyl and pyrimidyl rings rather than accepting hydrogen bonds from the amide is striking and contrary to the assumptions which have previously informed the design philosophy of MOF materials for CO₂ capture. Upon increasing the guest loading to 2.3 CO₂/Cu(II), the occupancy of site A nears saturation (0.96) and remains distinctly higher

than that of remaining sites B–H (range 0.50–0.18). In the structure of MFM-136 loaded with 1.1 CD₄/Cu(II), an equivalent site to site A in the center of the triangular pocket (C1A_{CD₄}···ring centroid = 4.33(2) Å) is observed to have the highest occupancy of 0.36. Additional CD₄ binding sites with lower occupancies were observed without notable interaction to the MOF host (Figure S19). To date, crystallographic characterizations of adsorbed gas molecules in MOFs have been mostly limited to one or two binding sites for materials with narrow pores.^{3–6} Simultaneous refinement of a large number of sites as reported in this work is made possible by the neutron diffraction data which give equal prominence to the light guests (particularly for CD₄) and heavy framework.

The absence of adsorbed CO₂ molecules at the pendant amide group could be due to the transition between “dynamic” and “kinetic” products in which the adsorbed CO₂ has great mobility to translate/diffuse along the pore and form interactions with amide groups in a “come and go” fashion. The static crystallographic experiment can only paint a picture averaged over an extended time scale. Hence, only more stable environments of CO₂ can be seen from the diffraction study. Thus, to gain direct insight into the binding dynamics of adsorbed CO₂ molecules and the free amide groups, inelastic neutron spectroscopy (INS) was measured for MFM-136 as a function of CO₂ loading (Figure 4). INS spectra for the bare MOF show multiple features which have been identified via DFT calculations (Figure S20). Specifically, the peak at 69 meV corresponds to the out-of-plane wagging modes of the N–H group, and peaks around 110–160 meV originate from the motion of aromatic C–H groups and deformational modes of

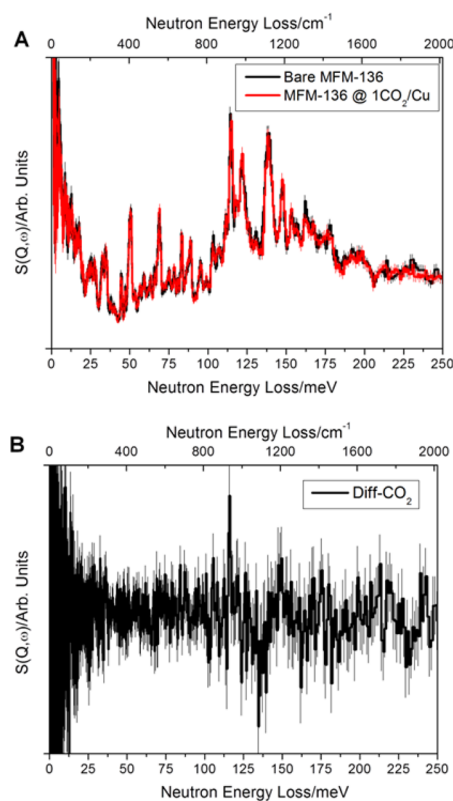


Figure 4. (a) Overlay of the INS spectra for bare and CO₂-loaded MFM-136; (b) difference INS spectrum for the bare and CO₂-loaded MFM-136.

the phenyl rings. Comparison of the INS spectra for bare and CO₂-loaded MFM-136 shows very small changes to the overall vibrational peaks except for a guest–host stiffening effect as evidenced by a global shift of peaks to slightly higher energy. Indeed, the N–H motion (69 meV) has no detectable changes upon CO₂ loading, while the aromatic C–H groups show small changes as confirmed by the difference spectra (Figure 4b), including a small increase in intensity at 116 meV (assigned as out-of-plane C–H bending on the isophthalate ring) and a decrease at 136 meV (assigned as in-plane C–H bending on all phenyl rings). This result is in excellent agreement with the NPD study and reaffirms the conclusion made from the diffraction experiment that direct CO₂ binding to the amide groups in the pore is absent.

Analysis of the CO₂-MOF interaction energy landscape determined during the GCMC simulation of the isotherm shows that the strongest predicted guest adsorption locations are in agreement with site A, followed by sites around the periphery of cage A corresponding to sites B–E (Figure S21). As in the NPD and INS studies, no strong adsorption was observed in the regions surrounding the N–H group.

In summary, a (3,6)-connected pyrimidyl isophthalate acylamide decorated MOF with a rare *eea*-topology has been synthesized. The amide-functionalized MOF exhibits high CO₂ uptake capacities and selectivity over CH₄ and N₂. Although it was anticipated that the amide moieties would actively participate in gas adsorption, the NPD and INS data reveal otherwise. The strongest binding site for both adsorbed CO₂ and CD₄ molecules are at the phenyl-isophthalate rings, and there is an absence of direct binding between adsorbed gas molecules and the pendent amide group in the pore. This has been confirmed by INS which shows retention of vibrational motion of the amide group upon CO₂ binding. This study indicates that introduction of functional groups in MOF structures may not necessarily result in the formation of strong binding sites for gas molecules. Future investigation of the impact of a combination of functional groups and pore geometry is currently underway.

■ ASSOCIATED CONTENT

Supporting Information

The Supporting Information is available free of charge on the ACS Publications website at DOI: 10.1021/jacs.6b08059.

Synthesis procedures, characterization, and additional analysis of crystal structures (CCDC-1452775, -1481608–1481610, and -1504702 contain the supplementary crystallographic data for this paper) (PDF) Crystallographic data (CIF)

■ AUTHOR INFORMATION

Corresponding Authors

*Sihai.Yang@manchester.ac.uk

*M.Schroder@manchester.ac.uk

Notes

The authors declare no competing financial interest.

■ ACKNOWLEDGMENTS

We thank EPSRC, ERC, Universities of Manchester and Nottingham for funding. O.B. thanks Niger Delta University and TETFund, Nigeria for a PhD scholarship. We thank STFC/ISIS for access to Beamlines TOSCA and WISH and providing computing resources on SCARF computer cluster.

We thank Drs S. Rudić and D. Khalyavin for help at ISIS. E.B. acknowledges access to the High Performance Computing Facility at the University of Nottingham.

■ REFERENCES

- (1) Allendorf, M. D.; Stavila, V. *CrystEngComm* **2015**, *17*, 229.
- (2) Guillermin, V.; Kim, D.; Eubank, J. F.; Luebke, R.; Liu, X.; Adil, K.; Lah, M. S.; Eddaoudi, M. *Chem. Soc. Rev.* **2014**, *43*, 6141.
- (3) (a) Bloch, E. D.; Queen, W. L.; Krishna, R.; Zdrozny, J. M.; Brown, C. M.; Long, J. R. *Science* **2012**, *335*, 1606. (b) Xiang, S.; Zhou, W.; Zhang, Z.; Green, M. A.; Liu, Y.; Chen, B. *Angew. Chem., Int. Ed.* **2010**, *49*, 4615. (c) Queen, W. L.; Hudson, M. R.; Bloch, E. D.; Mason, J. A.; Gonzalez, M. I.; Lee, J. S.; Gygi, D.; Howe, J. D.; Lee, K.; Darwish, T. A.; James, M.; Peterson, V. K.; Teat, S. J.; Smit, B.; Neaton, J. B.; Long, J. R.; Brown, C. M. *Chem. Sci.* **2014**, *5*, 4569.
- (4) Vaidhyanathan, R.; Iremonger, S. S.; Shimizu, G. K. H.; Boyd, P. G.; Alavi, S.; Woo, T. K. *Science* **2010**, *330*, 650.
- (5) (a) Lin, X.; Telepeni, I.; Blake, A. J.; Dailly, A.; Brown, C. M.; Simmons, J. M.; Zoppi, M.; Walker, G. S.; Thomas, K. M.; Mays, T. J.; Hubberstey, P.; Champness, N. R.; Schröder, M. *J. Am. Chem. Soc.* **2009**, *131*, 2159. (b) Yan, Y.; Yang, S.; Blake, A. J.; Schröder, M. *Acc. Chem. Res.* **2014**, *47*, 296.
- (6) Yang, S.; Ramirez-Cuesta, A. J.; Newby, R.; Garcia-Sakai, V.; Manuel, P.; Callear, S. K.; Campbell, S. I.; Tang, C. C.; Schröder, M. *Nat. Chem.* **2014**, *7*, 121.
- (7) (a) Li, B.; Zhang, Z.; Li, Y.; Yao, K.; Zhu, Y.; Deng, Z.; Yang, F.; Zhou, X.; Li, G.; Wu, H.; Nijem, N.; Chabal, Y. J.; Lai, Z.; Han, Y.; Shi, Z.; Feng, S.; Li, J. *Angew. Chem., Int. Ed.* **2012**, *51*, 1412. (b) Du, L.; Yang, S.; Xu, L.; Min, H.; Zheng, B. *CrystEngComm* **2014**, *16*, 5520. (c) Lee, C. H.; Huang, H. Y.; Liu, Y. H.; Luo, T. T.; Lee, G. H.; Peng, S. M.; Jiang, J. C.; Chao, I.; Lu, K. L. *Inorg. Chem.* **2013**, *52*, 3962. (d) Vaidhyanathan, R.; Iremonger, S. S.; Shimizu, G. K. H.; Boyd, P. G.; Alavi, S.; Woo, T. K. *Angew. Chem., Int. Ed.* **2012**, *51*, 1826.
- (8) (a) Alsmail, N. H.; Suyetin, M.; Yan, Y.; Cabot, R.; Krap, C. P.; Lu, J.; Easun, T. L.; Bichoutskaia, E.; Lewis, W.; Blake, A. J.; Schröder, M. *Chem. - Eur. J.* **2014**, *20*, 7317. (b) Zheng, B.; Bai, J.; Duan, J.; Wojtas, L.; Zaworotko, M. J. *J. Am. Chem. Soc.* **2011**, *133*, 748. (c) Zheng, B.; Yang, Z.; Bai, J.; Li, Y.; Li, S. *Chem. Commun.* **2012**, *48*, 7025. (d) Xiong, S.; He, Y.; Krishna, R.; Chen, B.; Wang, Z. *Cryst. Growth Des.* **2013**, *13*, 2670. (e) Chen, Y.-Q.; Qu, Y.-K.; Li, G.-R.; Zhuang, Z.-Z.; Chang, Z.; Hu, T.-L.; Xu, J.; Bu, X.-H. *Inorg. Chem.* **2014**, *53*, 8842. (f) Chen, Z.; Adil, K.; Weselinski, L. J.; Belmabkhout, Y.; Eddaoudi, M. *J. Mater. Chem. A* **2015**, *3*, 6276. (g) Lu, Z.; Bai, J.; Hang, C.; Meng, F.; Liu, W.; Pan, Y.; You, X. *Chem. - Eur. J.* **2016**, *22*, 6277.
- (9) Duan, J.; Yang, Z.; Bai, J.; Zheng, B.; Li, Y.; Li, S. *Chem. Commun.* **2012**, *48*, 3058.
- (10) Wei, Y.-S.; Lin, R.-B.; Wang, P.; Liao, P.-Q.; He, C.-T.; Xue, W.; Hou, L.; Zhang, W.-X.; Zhang, J.-P.; Chen, X.-M. *CrystEngComm* **2014**, *16*, 6325.
- (11) (a) Nandi, S.; De Luna, P.; Daff, T. D.; Rother, J.; Liu, M.; Buchanan, W.; Hawari, A. I.; Woo, T. K.; Vaidhyanathan, R. *Sci. Adv.* **2015**, *1*, e1500421. (b) Nugent, P.; Belmabkhout, Y.; Burd, S. D.; Cairns, A. J.; Luebke, R.; Forrest, K.; Pham, T.; Ma, S.; Space, B.; Wojtas, L.; Eddaoudi, M.; Zaworotko, M. J. *Nature* **2013**, *495*, 80.
- (12) Wang, J.; Huang, L.; Yang, R.; Zhang, Z.; Wu, J.; Gao, Y.; Wang, Q.; O'Hare, D.; Zhong, Z. *Energy Environ. Sci.* **2014**, *7*, 3478.
- (13) Singh, M. P.; Dhumal, N. R.; Kim, H. J.; Kiefer, J.; Anderson, J. A. *J. Phys. Chem. C* **2016**, *120*, 17323.
- (14) (a) Keceli, E.; Hemgesberg, M.; Grunker, R.; Bon, V.; Wilhelm, C.; Philippi, T.; Schoch, R.; Sun, Y.; Bauer, M.; Ernst, S.; Kaskel, S.; Thiel, W. R. *Microporous Mesoporous Mater.* **2014**, *194*, 115. (b) Debatin, F.; Thomas, A.; Kelling, A.; Hedin, N.; Bacsik, Z.; Senkovska, I.; Kaskel, S.; Junginger, M.; Mueller, H.; Schilde, U.; Jaeger, C.; Friedrich, A.; Holdt, H.-J. *Angew. Chem., Int. Ed.* **2010**, *49*, 1258.